Parisite-(La), ideally $CaLa_2(CO_3)_3F_2$, a new mineral from Novo Horizonte, Bahia, Brazil.

Luiz A. D. Menezes Filho[1],
Mario L. S. C. Chaves[1],
Nikita V. Chukanov[2],
Daniel Atencio[3],
Ricardo Scholz[4],
Igor Pekov[5],
Geraldo Magela da Costa[6],
Shaunna M. Morrison[7],
Marcelo B. Andrade[8],
Erico T.F. Freitas[9],
Robert T. Downs[7],
Dmitriy I. Belakovskiy[10]

[1]Universidade Federal de Minas Gerais (UFMG), Instituto de Geociências, Departamento de Geologia, Avenida Antônio Carlos, 6627, 31270-901, Belo Horizonte, MG, Brazil
[2]Institute of Problems of Chemical Physics, Russian Academy of Sciences, Chernogolovka, Moscow region, 142432 Russia
[3]Universidade de São Paulo, Instituto de Geociências, Rua do Lago 562, 05508-080, São Paulo, Brazil
[4]Universidade Federal de Ouro Preto (UFOP), Escola de Minas, Departamento de Geologia, Campus Morro do Cruzeiro, 35400-000, Ouro Preto, MG, Brazil
[5]Faculty of Geology, Moscow State University, Vorobievy Gory, Moscow, 119991 Russia
[6]Universidade Federal de Ouro Preto (UFOP), Instituto de Ciências Exatas e Biológicas, Departamento de Química, Campus Morro do Cruzeiro, 35400-000, Ouro Preto, MG, Brazil
[7]Department of Geosciences, University of Arizona, 1040 E. 4th Street, Tucson, Arizona 85721, U.S.A.

[8]University of São Paulo, São Carlos Institute of Physics, PO Box 369, 13560-970, São Carlos, SP, Brazil
[9]Universidade Federal de Minas Gerais (UFMG), Centro de Microscopia, Avenida Antônio Carlos, 6627, 31270-901, Belo Horizonte, MG, Brazil
[10]Fersman Mineralogical Museum of Russian Academy of Sciences, Leninskiy Prospekt 18-2, Moscow, 119071 Russia

ABSTRACT

Parisite-(La) (IMA number 2016-031), ideally $CaLa_2(CO_3)_3F_2$, occurs in a hydrothermal vein crosscutting a metarhyolite of the Rio dos Remédios Group, at the Mula mine, Tapera village, Novo Horizonte county, Bahia, Brazil, associated with hematite, rutile, almeidaite, fluocerite-(Ce), brockite, monazite-(La), rhabdophane-(La), and bastnäsite-(La). Parisite-(La) occurs as residual nuclei (up to 5 mm) in steep doubly-terminated pseudo-hexagonal pyramidal crystals (up to 8.2 cm). Parisite-(La) is transparent, yellow-green to white, with white streak, and displays a vitreous (when yellow-green) to dull (when white) lustre. Cleavage is distinct on pseudo-{001}; fracture is laminated, conchoidal, or uneven. The Mohs hardness is 4 to 5, and it is brittle. Calculated density is 4.273 g cm^{-3}. Parisite-(La) is pseudo-uniaxial (+), $\omega = 1.670(2)$, $\varepsilon = 1.782(5)$ (589 nm). The empirical formula normalized on the basis of 11 (O + F) *pfu* is $Ca_{0.98}(La_{0.83}Nd_{0.51}Ce_{0.37}Pr_{0.16}Sm_{0.04}Y_{0.03})_{\Sigma=1.94}C_{3.03}O_{8.91}F_{2.09}$. The IR spectrum confirms the absence of OH groups. Single-crystal X-ray studies gave the following results: monoclinic (pseudo-trigonal), space group: *C*2, *Cm*, or *C*2/*m*, a = 12.356(1) Å, b = 7.1368(7) Å, c = 28.299(3) Å, $\beta = 98.342(4)^{\circ}$, V = 2469.1(4) $Å^3$, Z = 12. Parisite-(La) is the La-dominant analogue of parisite-(Ce).

Keywords: Parisite-(La), new mineral, rare-earth fluorocarbonate, Mula mine, Novo Horizonte, Bahia, Brazil

INTRODUCTION

Parisite-(La) is the La-dominant analogue of parisite-(Ce). Minerals with a chemical composition consistent with that of parisite-(La) were reported in several studies from different localities: Třebíč durbachite massif, SW Moravia, Czech Republic (Sulovský 2001); at a metabauxite/marble interface in the eastern part of Samos island, Greece (Theye et al. 2003); alkaline rocks in Romania (Hirtopanu 2006, Hirtopanu et al. 2015); Cerro Boggiani massif, Alto Paraguay Province, Paraguay (Enrich et al. 2010); Bear Lodge carbonatite, Wyoming, USA (Moore et al. 2015). Parisite-(Nd) is also reported in literature as a mineral without IMA approval (Jambor et al. 1988).

Parisite-(La) has been approved as a new mineral species by the Commission of New Minerals, Nomenclature and Classification (CNMNC) of the International Mineralogical Association (IMA 2016-031). The type specimen of parisite-(La) is deposited in the mineralogical collection of the Museu de Geociências, Instituto de Geociências, Universidade de São Paulo, Rua do Lago, 562, 05508-080 - São Paulo, SP, Brazil, with the registration number DR1032 (a part of the holotype), and at the University of Arizona Mineral Museum (RRUFF Project deposition # R130687).

OCCURRENCE

Parisite-(La) occurs in a late-stage hydrothermal vein crosscutting metarhyolites, at the Mula mine, Tapera village, Novo Horizonte, State of Bahia, Brazil (12°48'28"S; 42°10'04"W). The metarhyolites, together with metadacites and meta-andesites, constitute the Rio dos Remédios Group, a package of metavolcanic acid rocks formed as a result of peraluminous and alkaline magmatism during a continental rift which opened ~1.75 Ga (Teixeira 2005, Martins et al. 2008). This group crops out in an area of about 35 × 10 km^2 and is one of the lithologic members of a larger package of metasedimentary and locally metavolcanic rocks called Serra do Espinhaço that extends N-S for about 1200 km from the center of Minas Gerais to the northern reaches of Bahia state (Figure 1). The evolution of the sedimentary basin in this region occurred in several stages during the Mesoproterozoic (~1.7-1.2 Ga) and during subsequent

metamorphism, folding and fracturing, during the Brasiliano Cycle of the Neoproterozoic (630 - 490 Ma, according to Pedrosa-Soares et al. 2011). During the Brasiliano event, swarms of hydrothermal quartz veins were generated. These have been exploited at Novo Horizonte for the production of rutilated quartz, barite and gold. Martins et al. (2008) reported muscovite ages of 404 and 490 Ma in altered metarhyolites close to these veins, confirming their formation during the Brasiliano event. Parisite-(La) is associated with almeidaite (its type locality is also the Mula mine: Menezes Filho et al. 2015), hematite, rutile, fluocerite-(Ce), brockite, monazite-(La), rhabdophane-(La) and bastnäsite-(La). The pit of the Mula mine is composed of brecciated quartz veins cemented by chalcedony. The veins show a stockwork pattern, which is typical of hydraulic fracturing processes, and are partially kaolinized; their orientation is NNW-SSE, with a thickness of up to 2 m.

APPEARANCE and PHYSICAL PROPERTIES

Parisite-(La) occurs as residual nuclei (up to 5 mm) in doubly-terminated pseudo-hexagonal pyramidal crystals (up to 8.2 cm) with corrugated faces (Figure 2a). The crystals apparently do not differ from what is usually described for parisite-(Ce): acute dipyramids with horizontally striated faces, terminated by pinacoid. The pinacoid faces are cleavage planes. The crystals are prismatic in appearance due to oscillatory combination of steep pyramids, but true prism faces are lacking or very small. However real forms of parisite-(La) can be pedion, pinacoid and sphenoid if the space group is *C*2, pedion, pinacoid and dome if *Cm*, pinacoid and prism if *C*2/*m*.These crystals were partially replaced by bastnäsite-(La), monazite-(La), and rhabdophane-(La). Crusts consisting of microcrystals of parisite-(La) also occur (Figure 2b).

Parisite-(La) is transparent, yellow-green to white, with white streak, and displays a vitreous (when yellow-green) to dull (when white) lustre. It is non-fluorescent under both shortwave (254 nm) and longwave (366 nm) ultraviolet radiation. Cleavage is distinct on pseudo-{001} and parting was not observed; fracture is laminated, conchoidal, or uneven. The Mohs hardness is between 4 and 5, and the mineral is brittle. Density was not measured; calculated density is 4.273 g cm^{-3} using the empirical formula. In transmitted light parisite-(La) is

colourless, pseudo-uniaxial (+), ω = 1.670(2), ε = 1.782(5) (589 nm). Pleochroism was not observed.

INFRARED and RAMAN SPECTROSCOPY

In order to obtain infrared (IR) absorption spectra, powdered samples were mixed with anhydrous KBr, pelletized, and analyzed using an ALPHA FTIR spectrometer (Bruker Optics) with the resolution of 4 cm^{-1} in the wavenumber range from 360 to 3800 cm^{-1}; 16 scans were obtained. The IR spectrum of an analogous pellet of pure KBr was used as a reference. The assignments of IR bands have been made in accordance with Adler and Kerr (1963), White (1974), and Nakamoto (1997, 2009).

The IR spectrum of parisite-(La) is close to that of parisite-(Ce) (Figure 3). Weak IR bands in the range 1700–3000 cm^{-1} correspond to overtones and combination modes. The other bands are assigned as follows (cm^{-1}; w – weak band, s – strong band, sh – shoulder): 1454s, 1430sh (degenerate asymmetric C–O-stretching vibrations), 1089w, 1081w (non-degenerate symmetric C–O-stretching vibrations), 871s, 850sh (out-of-plane bending vibrations of the carbonate ion triangles), 746w, 734w (in-plane bending vibrations of the carbonate ion triangles), 679w, 602w (presumably, overtones and/or combination modes), 368 (lattice mode involving Ca–O- or *REE*–O-stretching vibrations). Bands in the range 3000-3800 cm^{-1} are not observed, which indicates the absence of OH groups.

Raman spectrum of parisite-(La) (Figure 4) was collected on a randomly oriented crystal at 100% of 150 mW on a Thermo Almega microRaman system, using a 532 nm solid-state laser, confocal Olympus optics with a 10x objective, and a thermoelectrically cooled CCD detector. The laser was partially polarized with 4 cm^{-1} resolution and a spot size of 1 μm. The peak at 1428 cm^{-1} corresponds to the v_3 asymmetric stretching mode of CO_3^{2-} anions. Symmetric C–O stretching modes are represented by the bands at 1081, 1091, and 1098 cm^{-1}. The bands at 737 and 871 cm^{-1} correspond to in-plane and out-of-plane vibrations of CO_3^{2-}, respectively. The bands at 600 and 970 cm^{-1} may be due to any vibrations involving F^- anions. Bands with wavenumbers below 500 cm^{-1} are attributed to lattice modes. The tentative assignment of Raman bands is based on previous studies (Frost & Dickfos 2007, Guastoni et al. 2010, Frost et al.

2013). All peaks above 1500 cm-1 are due to fluorescence. This effect is typical for REE compounds (see e. g. Betancourtt 2003)

CHEMICAL DATA

Chemical analyses (25) were carried out using a Cameca SX100 microprobe (WDS mode, 25 kV, 40 nA, beam diameter 5 μm) at the Department of Geosciences, University of Arizona, Tucson, Arizona, U.S.A. H_2O was not analysed because of the absence of bands corresponding to O–H vibrations in the IR spectrum. The thermogravimetric (TG) curve of parisite-(La) in nitrogen atmosphere is given in Figure 5. The second step in the TG curve may be due to the decomposition of an intermediate carbonate. Fluorine is not lost during the heating because CaF_2 melts above 1400°C without decomposition and *REE*F_3 do not decompose into elements below 1200°C (Ranieri et al. 2008). The formula corresponding to CO_2 content of 23.68% obtained experimentally from TG data is is not charge balanced. This weight loss is slightly less than 24.50 wt% CO_2 calculated for formula neutrality. Mean analytical results are given in Table 1. The empirical formula normalized on the basis of 11 (O + F) *pfu* is $Ca_{0.98}(La_{0.83}Nd_{0.51}Ce_{0.37}Pr_{0.16}Sm_{0.04}Y_{0.03})_{\Sigma=1.94}C_{3.03}O_{8.91}F_{2.09}$, where CO_2 was constrained to 24.50% for charge neutrality. The idealized formula is $CaLa_2(CO_3)_3F_2$, which requires: La_2O_3 60.80, CaO 10.46, CO_2 24.63, F 7.09, O=F -2.98, total 100.00wt.%.

An additional sample was measured at the Instituto de Geociências, Universidade Federal de Minas Gerais, Belo Horizonte, Minas Gerais, Brazil. Chemical analyses (7) were carried out using a Jeol JXA8900R electron microprobe (WDS mode, 15 kV, 20 nA, beam diameter 5 μm). Mean analytical results are given in Table 1. The empirical formula normalized on the basis of 11 (O + F) *pfu* is $Ca_{0.91}(La_{0.82}Nd_{0.47}Ce_{0.43}Pr_{0.26}Sm_{0.04}Y_{0.02})_{\Sigma=2.04}(CO_3)_{3.03}F_{1.91}$, where CO_2 was constrained to 24.70% for charge neutrality.

CRYSTALLOGRAPHY

Single-crystal X-ray diffraction studies and Convergent-Beam Electron Diffraction (CBED) analysis performed under TEM indicated monoclinic symmetry (pseudo-trigonal) and systematic absences compatible with space groups *C*2(#5), *Cm*(#8), *C*2/*m* (#12). Single-crystal X-ray diffraction studies carried out using a Bruker APEX2 CCD automated diffractometer with graphite-monochromatized Mo*K*α (λ = 0.71073 Å) radiation gave the following results: *a* = 12.356(1) Å, *b* = 7.1368(7) Å, *c* = 28.299(3) Å, β = 98.342(4)º, *V* = 2469.1(4) Å^3, Z = 12. The *a : b : c* ratio calculated from the unit cell parameters is 1.7313 : 1 : 3.9652. Gladstone-Dale compatibility is -0.046 (good) for the chemical analysis made in Arizona and -0.032 (excellent) for the chemical analysis made in Minas Gerais.

We confirmed that the space groups *C*2/*c*(#15) and *Cc* (#9) cited by Ni et al. (2000) were not consistent for parisite-(La). The space group *C*2/*c* (#15) analysis show 816 reflections satisfying systematic absence conditions with an average I/s (I) of 2.07 (21518 reflections read) and for the space group *Cc* (#9), there are 789 reflections with an average I/s(I) of 2.11 at the same conditions (20612 reflections read).

For TEM studies, the sample was ground in an agate mortar and dispersed in a small volume (1 mL) of isopropanol. The suspension was dropped onto the carbon-coated Cu-TEM grid (300 mesh), and placed in a desiccator before TEM analysis. Convergent-Beam Electron Diffraction (CBED) and Nano-Beam Electron Diffraction (NBD) were performed by using a Tecnai G2-20 TEM (FEI), with LaB_6 filament, operated at 200 kV, at the Center of Microscopy at UFMG, Belo Horizonte, Brazil. The diffraction patterns were recorded by using a side-mounted ES500W Erlangshen CCD camera (Gatan). The CBED patterns were performed using a convergence semi-angle of 1.3 mrad, with a beam size of approximately 20 nm, and the NBD conditions were achieved by slightly spreading the C2 condenser lens to obtain a nearly parallel narrow beam.

In order to deduce the crystal system, the Bravais lattice, and the possible space group, electron diffraction experiments were carried out following Morniroli and Steeds (1992), Redjaïmia and Morniroli (1994), Jacob et al. (2012), and Morniroli (2013). A suitable area of the sample was illuminated by a focused narrow beam under the TEM. Observations of CBED patterns were done while the sample was being tilted around a chosen Kikuchi line, or a row containing reflections, which passed through the origin of the reciprocal lattice. Several zone axis patterns (ZAPs) were recorded in the CCD until the ZAP of highest “net”-symmetry had been

found. The “net”-symmetry takes into account the position of the reflections observed in the diffraction pattern, not their intensity. It is defined as the symmetry of the spots “net” displayed in the zeroth order Laue zone (ZOLZ) and the whole pattern (WP), which includes the ZOLZ and first order Laue zone (FOLZ) (Morniroli and Steeds 1992; Jacob et al. 2012). Following Morniroli and Steeds (1992), the “net”-symmetry is here referred as “(ZOLZ)WP” symmetry – the (ZOLZ) symmetry is put in brackets henceforth in order to distinguish it from the WP’s.

The identification of the monoclinic crystal system was achieved by observing the ZAP of highest “net”-symmetry shown in Figure 6. The two perpendicular axes drawn in the pattern (Figure 6) indicate 2 mirrors, and also 2-fold axes, for the spots net shown in the ZOLZ, therefore the symmetry is (2*mm*). The vertical axis shown in Figure 6, however, is not a mirror for the WP, but the horizontal one. So the “net”-symmetry observed in this ZAP is (2mm)m. Comparisons with the Atlas of Electron Diffraction Zone-Axis Pattern (Morniroli 2013) showed that the ZAP shown in Figure 6 corresponds to the [u0w] zone axis for the monoclinic system.

The non-primitive *mS* (*mA* or *mB*) Bravais lattice was deduced by comparing the features displayed in the diffraction pattern shown in Figure 7 with the typical ZAPs for the monoclinic crystal system (Morniroli 2013). The Figure 7.a shows the ZOLZ reflections of the either $[010]_b$ or $[001]_c$ zone axis, on which two symmetry axes are drawn – the subscripts b and c stand for unique axis b and c, respectively. These non-perpendicular axes (beta* or gamma* equal 89.18^o) indicate the 2-fold symmetry (2) for the spots net seen in the ZOLZ. The FOLZ reflections were not easily observed at first, so the electron beam was tilted along each axis until the FOLZ reflection could be seen at the microscope screen as shown in Figures 7.b and 7.c. From the observation of the FOLZ reflections the symmetry of the WP was taken as 2-fold. So the “net”-symmetry of this ZAP concluded as (2)2. This is the exact zone axis pattern required for the identification of the Bravais lattice for the monoclinic system (Morniroli 2013).

The narrow parallelograms drawn in the ZOLZ and FOLZ reflections shown in Figure 7 correspond to the “unit” cell in the reciprocal space. This “unit” cell indicates the periodicity of reflections in the spots net in the diffraction pattern. As can be seen in Figure 6, there is a relative shift of the “unit” cell in the FOLZ compared to the ZOLZ. It means that the Bravais lattice of the Parisite-(La) crystal is non-primitive (Morniroli and Steeds 1992; Jacob et al. 2012). Therefore, the Bravais lattice is *mS* (*mA* or *mB*).

The lack of periodicity differences between ZOLZ and FOLZ reflections is an evidence that there are no glide planes parallel to $[010]_b$ or $[001]_c$ (Morniroli and Steeds 1992; Jacob et al. 2012) as reported by Ni et al (2000) for parisite-(Ce). It was not possible to deduce the screw axis perpendicular to the zone axis pattern [u0w] shown in Figure 6. The possible 2_1 screw axis perpendicular to that particular zone axis could be related to the forbidden reflections in the row defined by any of the symmetry axes shown in Figure 6. The forbidden nodes would appear, however, due a double diffraction effect. This could be checked out by tilting the beam around the symmetry axis shown in Figure 6 in order to decrease the intensity of the likely forbidden reflections (Morniroli and Steeds 1992), but it has been not verified during measurements. Moreover, the absence of glide planes parallel to $[010]_b$ or $[001]_c$ are consistent with the possible extinction symbols, $A1\text{-}1_b$ or $B11\text{-}_c$. From the comparisons of the features observed in the experimental ZAPs with the typical theoretical diffraction patterns (Morniroli 2013), the possible space groups are *A*121 (#5), *A*1*m*1 (#8), *A*12/*m*1 (#12), *B*112 (#5), *B*11*m* (#8) or *B*112/*m* (#12), alternative settings of the space groups *C*2(#5), *Cm*(#8), *C*2/*m* (#12).

Unfortunately, despite determining monoclinic unit-cell parameters from the single-crystal pattern, we could not obtain single-crystal data suitable for the structure refinement. Thin inclusions are visible under the microscope. Possible they are the main cause of the absence of single crystals suitable for structural investigations. Inclusions of synchysite, röntgenite or bastnäsite microblocks are typical for parisite in general.

X-ray powder diffraction data (Table 2) were obtained using a Rigaku R-AXIS Rapid II single-crystal diffractometer equipped with cylindrical image plate detector using Debye-Scherrer geometry (d = 127.4 mm; Co$K\alpha$-radiation). Parameters of monoclinic unit cell refined from powder data are: a = 12.323(7), b = 7.121(2), c = 28.28(1) Å, β = 98.33(4)º, V = 2456(3) Å^3.

DISCUSSION

The second most abundant *REE* in parisite-(La) from Mula mine is Nd, not Ce. On a chondrite-normalized plot there would be a marked negative Ce anomaly. One hypothesis about the conditions of formation could be that the fluids that transported *REE* had leached them in a mildly oxidizing environment, where Ce was partially oxidized to Ce^{4+} and thus remained

immobile. The resulting solution would be depleted in Ce. For the other five parisite-(La) occurrences quoted in the literature, neither crystallographic nor chemical data are presented. The only exception is a partial chemical analysis for parisite-(La) from Třebíč durbachite massif, SW Moravia, Czech Republic (Sulovský 2001): La_2O_3 28.68, Ce_2O_3 24.07, Nd_2O_3 4.01, CaO 10.22, SO_3 0.98, F 6.38, O=F -2.67, total 71.64 wt.%. The calculated formula is $Ca_{1.01}(La_{0.97}Ce_{0.81}Nd_{0.13})_{\Sigma 1.91}(CO_3)_{2.89}(SO_4)_{0.07}F_{1.84}$. In this case Ce is the second most abundant *REE* and the conditions of formation differ from that of parisite-(La) from Mula mine.

ACKNOWLEDGEMENTS

We acknowledge the Brazilian agencies FAPESP (processes 2014/50819-9 and 2013/03487-8), CNPq, and Finep for financial support, all members of the IMA Commission on New Minerals, Nomenclature and Classification, the Principal Editor Peter Williams, the reviewers Fernando Colombo, Peter Leverett and an anonymous for their helpful suggestions and comments. M. Chaves thanks to CNPq (grant No. 305492/2013-6) and R. Scholz thanks to CNPq and FAPEMIG (respectively grant No. 305284/2015-0 and grant APQ-01448-15).

REFERENCES

Adler, H.H and Kerr, P.F. (1963) lnfrared spectra, symmetry and structure relations of some carbonate minerals. *American Mineralogist*, **48**, 839-853

Betancourtt, V.M.R. (2003) Raman Spectroscopic Study of High Temperature Rare Earth Metal - Rare Earth Halide Solutions: Ln-LnX_3- and LnX_2-LnX_3-$(LiX\text{-}KX)_{eu}$ Systems (Ln: Nd, Ce; X: Cl, I). Dr. Sci. thesis. Faculty of Chemistry and Biosciences, Karlsruhe University.

Cheang, K. (1977) Structure and Polytypism in Synchysite and Parisite from Mont St. Hilaire, Quebec. M.S. thesis, Carleton University, Ottawa, Canada.

Enrich, G.E.R., Gomes, C.B., and Ruberti, E. (2010) Química mineral de carbonatos de elementos terras raras em nefelina sienitos e fonólitos agpaíticos do maciço de Cerro

306 Boggiani, Província Alto Paraguay, Paraguai. In: X Congresso de Geoquímica dos Países de
307 Língua Portuguesa, 2010, Porto. Actas, 2010. v. CD-rom. p. 223-227.
308 Flink, G. (1901) Part I. On the minerals from Narsarsuk on the Firth of Tunugdliarfik in Southern
309 Greenland. Parisite. *Meddelelser om Grønland*, **24**, 29-42.
310 Frost, R.L. and Dickfos, M.J. (2007) Raman spectroscopy of halogen-containing carbonates
311 *Journal of Raman Spectroscopy*, **38**, 1516–1522.
312 Frost, R.L., López, A., Scholz, R., Xi, Y., and Belotti, F.M. (2013) Infrared and Raman
313 spectroscopic characterization of the carbonate mineral huanghoite – And in comparison
314 with selected rare earth carbonates. *Journal of Molecular Structure*, **1051**, 221-225.
315 Guastoni, A., Kondo, D., and Nestola, F. (2010) Bastnäsite-(Ce) and parisite-(Ce) from Mt.
316 Malosa, Malawi. *Gems & Gemology*, **46**, 42-46.
317 Hirtopanu, P. (2006) One hundred minerals for one hundred years (dedicated to the Centennial of
318 the Geological Institute of Romania), 3rd Conference on Mineral Sciences in the
319 Carpathians, Miskolc Hungary. *Acta Mineralogica-Petrographica, Abstract series*, **5**, 86.
320 Hirtopanu, P., Fairhurst, R.J., and Jakab, G. (2015) Niobian rutile and its associations at Jolotca,
321 Ditrau Alkaline Intrusive Massif, East Carpathians, Romania. *Proceedings of the Romanian*
322 *Academy, Series* B, **17**, 39–55.
323 Jacob, D., Ji, G., and Morniroli, J.P. (2012) A systematic method to identify the space group from
324 PED and CBED patterns part II--practical examples. *Ultramicroscopy*, **121**, 61–71.
325 Jambor, J.L., Burke, E.A., Ercit, T.S, and Grice, J.D. (1988) New mineral names. *American*
326 *Mineralogist*, **73**, 1496-1497.
327 Martins, A.A.M., Andrade Filho, E.L.A, Loureiro, H.S.C., Arcanjo, J.B.A., and Guimarães,
328 R.V.B. (2008) Geologia da Chapada Diamantina Oriental (Projeto Ibitiara - Rio de Contas) -
329 Série Arquivos Abertos 31 - CPRM (Serviço Geológico do Brasil) and CBPM (Companhia
330 Baiana de Pesquisa Mineral), Salvador, 64 pp.
331 Menezes Filho, L.A.D., Chukanov, N.V., Rastsvetaeva, R.K., Aksenov, S.M., Pekov, I.V.,
332 Chaves, M.L.S.C., Richards, R.P., Atencio, D., Brandão, P.R.G., Scholz, R., Krambrock, K.,
333 Moreira, R.L., Guimarães, F.S., Romano, A.W., Persiano, A.C., Oliveira, L.C.A., and
334 Ardisson, J.D. (2015) Almeidaite, $Pb(Mn,Y)Zn_2(Ti,Fe^{3+})_{18}O_{36}(O,OH)_2$, a new crichtonite-
335 group mineral, from Novo Horizonte, Bahia, Brazil. *Mineralogical Magazine*, **79**, 269–283

Moore, M., Chakhmouradian, A.R., Mariano, A.N., and Sidhu, R. (2015) Evolution of rare-earth mineralization in the Bear Lodge carbonatite, Wyoming: Mineralogical and isotopic evidence. *Ore Geology Reviews*, **64**, 499-521.

Morniroli, J.P. (2013) *Atlas of Electron Diffraction Zone Axis Patterns*, p. 314. Available at: http://www.electron-diffraction.fr.

Morniroli, J.P. and Steeds, J.W. (1992) Microdiffraction as a tool for crystal structure identification and determination. *Ultramicroscopy*, **45**, 219–239.

Nakamoto, K. (1997) Infrared and Raman Spectra of Inorganic and Coordination Compounds. Part A: Theory and Applications in Inorganic Chemistry. John Wiley and Sons, New York.

Nakamoto, K. (2009) Infrared and Raman Spectra of Inorganic and Coordination Compounds. Part A: Theory and Applications in Inorganic Chemistry. (Sixth edition). John Wiley and Sons, New Jersey.

Ni, Y, Post, J.E. and Hughes, J.M. (2000) The crystal structure of parisite-(Ce), $Ce_2CaF_2(CO_3)_3$. *American Mineralogist*, **85**, 251-258.

Pedrosa-Soares, A.C., Campos, C., Noce, C.M., Silva, L.C., Novo, T., Roncato, J., Medeiros, S., Castañeda, C., Queiroga, G., Dantas, E., Dussin, I., and Alkmim, F. (2011) Late Neoproterozoic-Cambrian granitic magmatism in the Araçuaí orogen (Brazil), the Eastern Brazilian Pegmatite Province and related deposits. *Geological Society of London Special Publications*, **350,** 25-51.

Ranieri, I.M., Baldochi, S.L., and Klimm, D.(2008) The Phase Diagram GdF_3–LuF_3. *Journal of Solid State Chemistry*, **181(5)**, 1070-1074.

Redjaïmia, A. and Morniroli, J.P. (1994) Application of microdiffraction to crystal structure identification. *Ultramicroscopy*, **53**, 305–317.

Sulovský, P. (2001) Accessory minerals of the Třebíč durbachite massif (SW Moravia). *Mineralia Slovaca, Košice: SGS*, **33(5)**, 467-472.

Teixeira, L.R. (2005) Projeto Ibitiara - Rio de Contas, Estado da Bahia. Programa Recursos Minerais do Brasil, Litogeoquímica, CPRM (Serviço Geológico do Brasil) and CBPM (Companhia Baiana de Pesquisa Mineral), Salvador, 33 pp. + xv.

Theye, T., Ockenga, E., and Bertoldi, C. (2003) Davidite(-La), bastnaesite(-La), parisite(-La), monazite(-La): REE minerals at a metabauxite/marble interface in eastern Samos (Greece). Berichte der Deutschen Mineralogischen Gesellschaft, Beihefte zum European Journal of

Mineralogy Vol. 15, No. 1. ftp://ftp.gmg.rub.de/pub/geo2003/17%20Quantification%20and%20dating%20of%20metamorphic%20processes%20WILLNER/Theye.PDF

White, W.B. (1974) The carbonate minerals. In: (Farmer, V.C., ed.) Infrared spectra of minerals. *Mineralogical Society Monography*, **4**, 227-284.

Table 1. Chemical data for parisite-(La).

	1					
constituent	wt.%	range	stand. dev.	probe standard	xtal	line
CaO	10.10	10.05-10.15	0.02	wollastonite	PET	Kα
Y_2O_3	0.52	0.47-0.55	0.02	YAG	TAP	Lα
La_2O_3	24.77	24.54-24.96	0.11	REE3	LIF	Lα
Ce_2O_3	11.16	11.03-11.32	0.07	REE3	LIF	Lα
Pr_2O_3	4.73	4.63-4.91	0.06	REE3	LIF	Lβ
Nd_2O_3	15.82		0.09	REE2	LIF	Lβ
Sm_2O_3	1.25		0.03	REE2	LIF	Lβ
Eu_2O_3	0.07		0.03	REE1	LIF	Lβ
F	7.30		0.18	MgF_2	TAP	Kα
CO_2	(24.50)			(calculated)*		
–O=F	– 3.07	-	-			
Total	97.15					

	2					
constituent	wt.%	range	stand. dev.	probe standard	xtal	line
CaO	9.45	9.28 – 9.73	0.16	wollastonite	PETJ	Kα
Y_2O_3	0.51	0.48 – 0.54	0.02	YAG	TAP	Lα
La_2O_3	24.82	24.31 – 25.32	0.41	monazite-(Ce)	PETJ	Lα
Ce_2O_3	12.99	12.86 – 13.24	0.16	monazite-(Ce)	PETJ	Lα
Pr_2O_3	7.95	7.27 – 8.83	0.53	monazite-(Ce)	LIF	Lβ
Nd_2O_3	14.77	14.23 – 15.26	0.38	monazite-(Ce)	LIF	Lβ
Sm_2O_3	1.24	1.22 – 1.27	0.02	monazite-(Ce)	LIF	Lβ
Eu_2O_3	0.07	0.02 – 0.09	0.03	monazite-(Ce)	LIF	Lβ
F	6.71	6.01 – 7.58	0.48	MgF_2	TAP	Kα
CO_2	(24.70)	-	-	(calculated)*		
–O=F	– 2.82	-	-			
Total	100.39					

1. Analyses at the Department of Geosciences, University of Arizona, Tucson, Arizona, U.S.A.
2. Analyses at the Instituto de Geociências, Universidade Federal de Minas Gerais, Belo Horizonte, Minas Gerais, Brazil.

*calculated from the idealized formula.
Probe standard composition:
YAG = Y : 44.93%, Al: 22.73%, O: 32.34%
REE1 = Si: 12.60%, Al: 16.15%, Ca: 17.98%, Eu: 3.8%, Gd: 3.87%, Tb: 3.78%, Tm: 3.81%, O: 38.01%
REE2 = Si: 12.65%, Al: 16.21%, Ca: 18.05%, Nd: 3.65%, Sm: 3.67%, Yb: 3.74%, Lu: 3.75%, O: 38.27%
REE3 = Si: 12.69%, Al: 16.26%, Ca: 18.1%, Y : 3.21%, La: 3.65%, Ce: 3.42%, Pr: 3.79%, O: 38.88%

Table 2. Powder X-ray diffraction data of parisite-(La).

I_{obs}	d_{obs}, Å	d_{calc}, Å	*h k l**
55	13.95	13.991	002
20	6.98	6.995	004
37	4.655	4.664	006
88	3.555	3.561, 3.558	020, -311
13	3.446	3.451, 3.449, 3.448	022, 311, -313
3	3.323	3.326, 3.325, 3.324	023, 312, -314
18	3.169	3.173, 3.172, 3.171	024, 313, -315
12	3.000	3.004, 3.003, 3.002	025, 314, -316
100	2.827	2.830, 2.829, 2.828	026, 315, -317
2	2.655	2.659, 2.658, 2.657, 2.657	027, 316, -318, 404
2	2.495	2.495, 2.495, 2.494	028, 317, -319
8	2.331	2.332	0.0.12
1	2.274	2.275, 2.274, 2.271	-133, -424, -229
2	2.241	2.246, 2.245	133, 422
10	2.199	2.200, 2.200, 2.199	0.2.10, 319, -3.1.11
58	2.055	2.055, 2.054	-331, -602
4	2.034	2.033, 2.032, 2.032	-333, 600, -604
6	1.971	1.972, 1.972, 1.971, 1.971	333, -335, 602, -606
38	1.950	1.951, 1.951, 1.950	0.2.12, 3.1.11, -3.1.13
36	1.880	1.881, 1.881, 1.880, 1.879	335, -337, 604, -608
9	1.780	1.780, 1.779	040, -622
2	1.767	1.772, 1.772, 1.771	337, -339, -6.0.10
1	1.749	1.749	0.0.16
3	1.725	1.725, 1.724, 1.724	044, 622, -626
23	1.663	1.663, 1.662, 1.662	046, 624, -628
3	1.570	1.570, 1.570, 1.569	0.2.16, 3.1.15, -3.1.17
12	1.542	1.542, 1.542, 1.542, 1.541	3.3.11, -3.3.13, 6.0.10, -6.0.14
2	1.502	1.502, 1.502, 1.501	0.4.10, 628, -6.2.12
9	1.425	1.425, 1.425, 1.424	0.2.18, 3.1.17, -3.1.19
9	1.415	1.415, 1.415, 1.414	0.4.12, 6.2.10, -6.2.14
9	1.346	1.346, 1.345, 1.345	-351, -642, -913
3	1.332	1.332, 1.332, 1.332	3.3.15, 6.0.14, -3.3.17

*The *hkl* indices are chosen taking into account intensities of reflections of the powder X-ray diffraction pattern calculated from the structure data for monoclinic parisite-(Ce) reported by Ni et al. (2000).

446 Table 3. Comparative data for parisite-(La) and parisite-(Ce).

	Parisite-(La)	Parisite-(Ce)
Formula	$CaLa_2(CO_3)_3F_2$	$CaCe_2(CO_3)_3F_2$
Space group	*C*2, *Cm*, *C*2/*m*	*C*2/*c* or *Cc*
a, Å *b*, Å *c*, Å *Z*	*a* = 12.3563(13) *b* = 7.1368(7) *c* = 28.299(3) Å β = 98.342(4)º Z = 12	*a* = 12.305(2) *b* = 7.1053(5) *c* = 28.250(5) β = 98.257(14)° Z = 12
Strong lines of the X-ray powder-diffraction pattern: *d*, Å (*I*, %)	2.827 (100), 3.555 (88), 2.055 (58), 13.95 (55), 1.950 (38), 4.655 (37), 1.880 (36)	3.565 (100), 2.838 (100), 2.060 (80), 1.938 (60), 1.882 (50), 1.658 (50), 14.03 (40)
Optical data: ω ε Optical sign	 1.670(2) 1.782(5) (+)	 1.6718–1.6767 1.7664–1.7729 (+)
Density, $g \cdot cm^{-3}$	4.331	4.3915
Mohs hardness	4 - 5	4 ½
References	This study	Cell data: Ni et al. (2000); XRPD: Cheang (1977); optical data, density, hardness: Flink (1901)

447

448

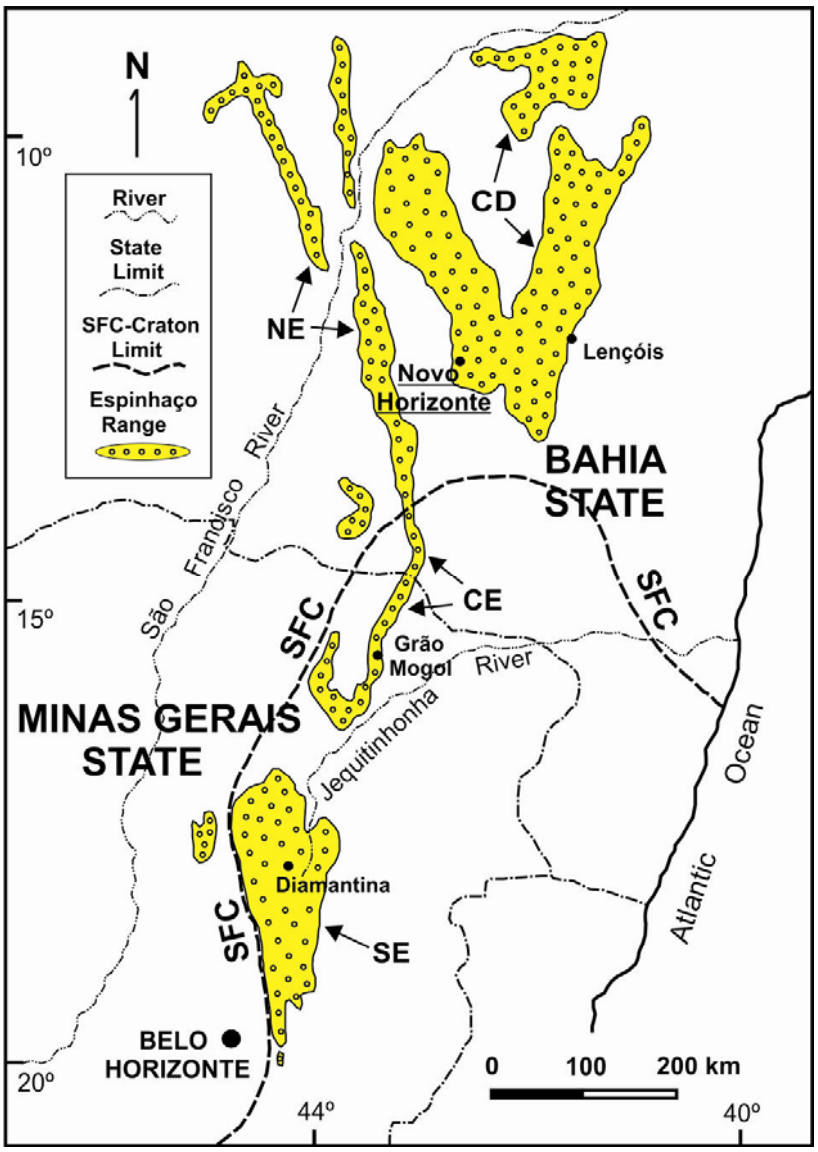

Figure 1. The Espinhaço Range in Eastern Brazil (states of Bahia and Minas Gerais), showing its geographic/geotectonic domains Southern Espinhaço (SE), Central Espinhaço (CE), Northern Espinhaço (NE) and Chapada Diamantina (CD) in relation to the São Francisco Craton (SFC). The study area near Novo Horizonte (Bahia) is underlined.

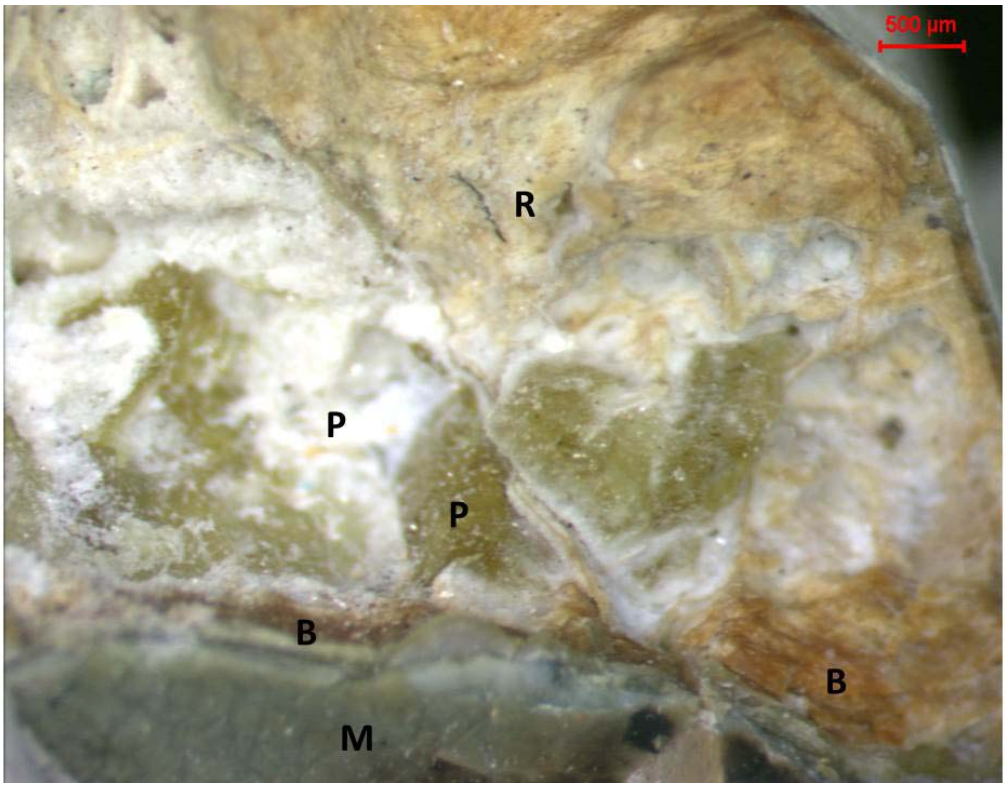

Figure 2a – Partial pseudomorphs of monazite-(La) [M], bastnäsite-(La) [B], and rhabdophane-(La) [R] after parisite-(La) [P].

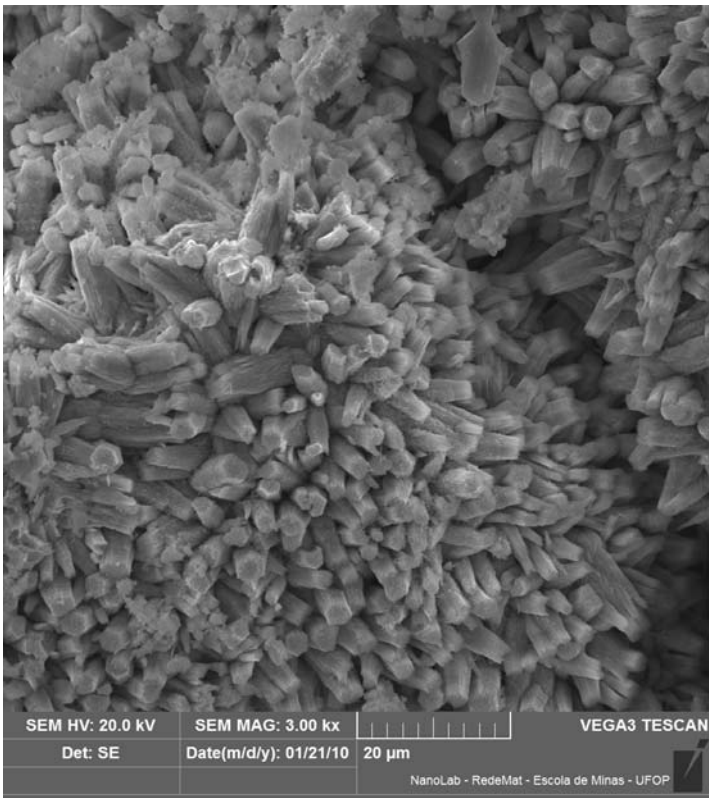

Figure 2b – Crust consisting of microcrystals of parisite-(La).

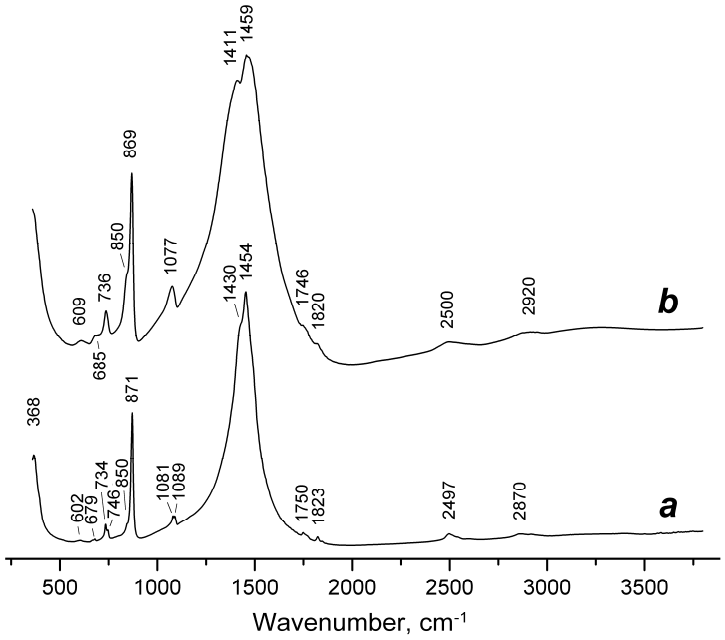

Figure 3. Powder infrared spectra of (*a*) parisite-(La) and (*b*) parisite-(Ce) with the empirical formula $Ca_{1.08}(Ce_{0.93}La_{0.47}Nd_{0.32}Pr_{0.06}Y_{0.08}Th_{0.06})_{\Sigma=1.92}(CO_3)_{3.00}F_{1.88}$ from White Cloud Mine, Pyrites, Ravalli Co., Montana, USA.

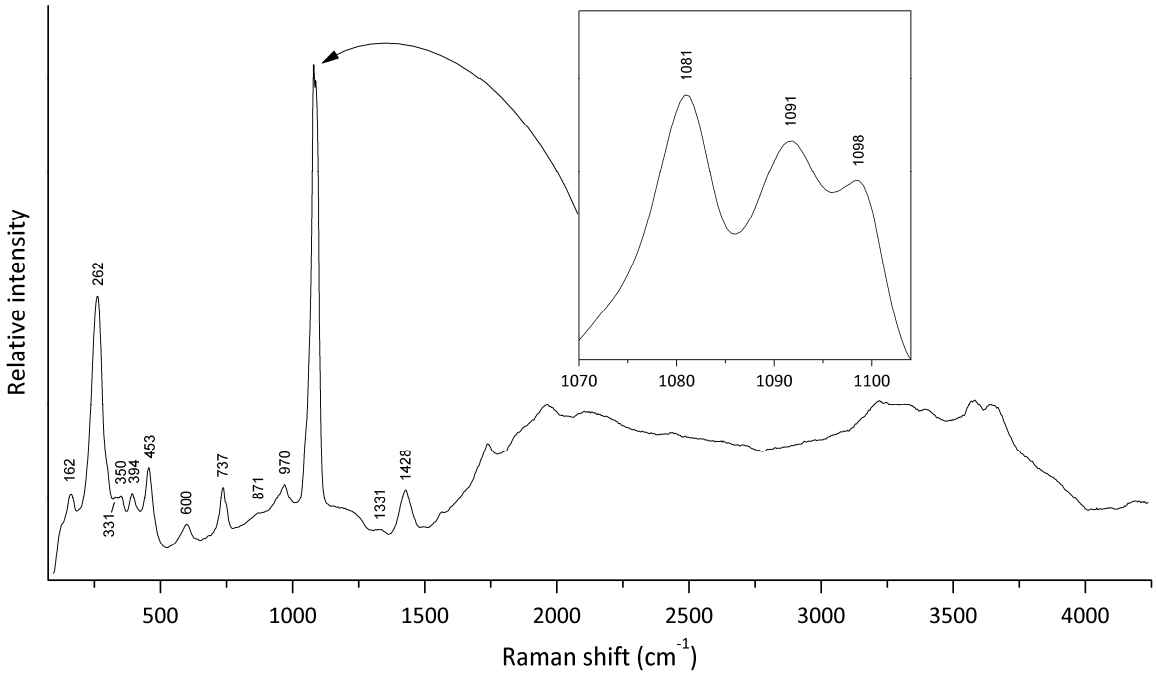

Figure 4 – Raman spectrum of parisite-(La).

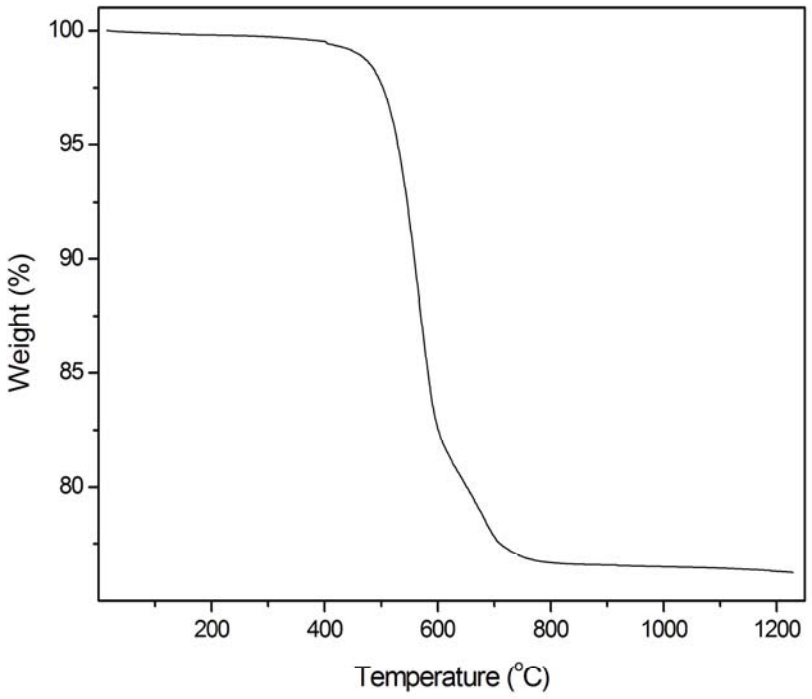

Figure 5. TG curve of parisite-(La).

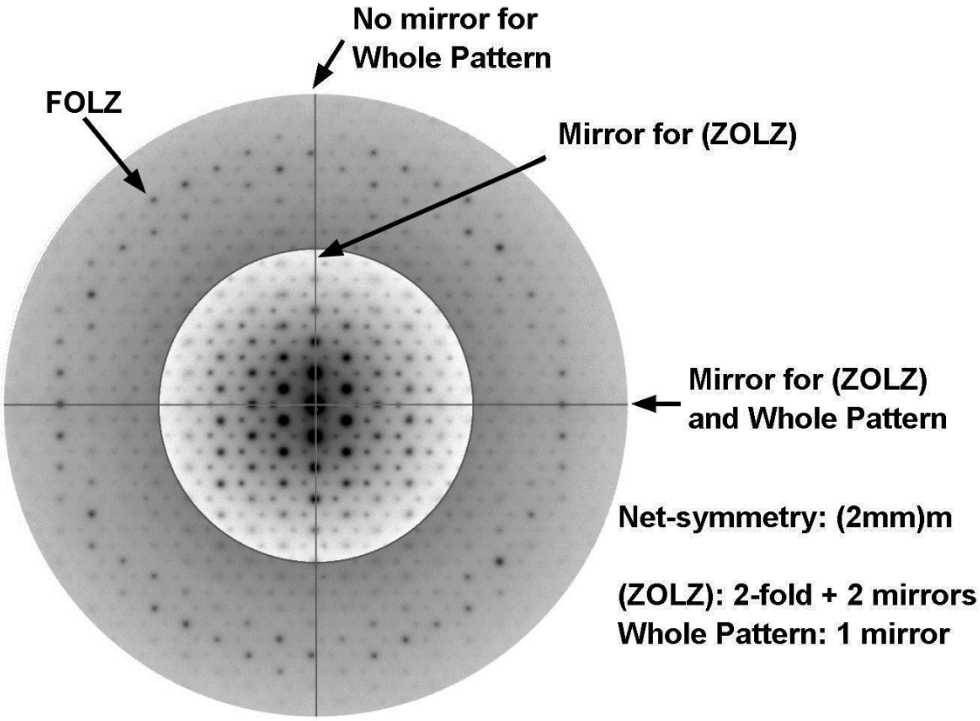

Figure 6 – Electron diffraction zone axis pattern of highest "net"-symmetry found in parisite-(La), required for the identification of the crystal system.

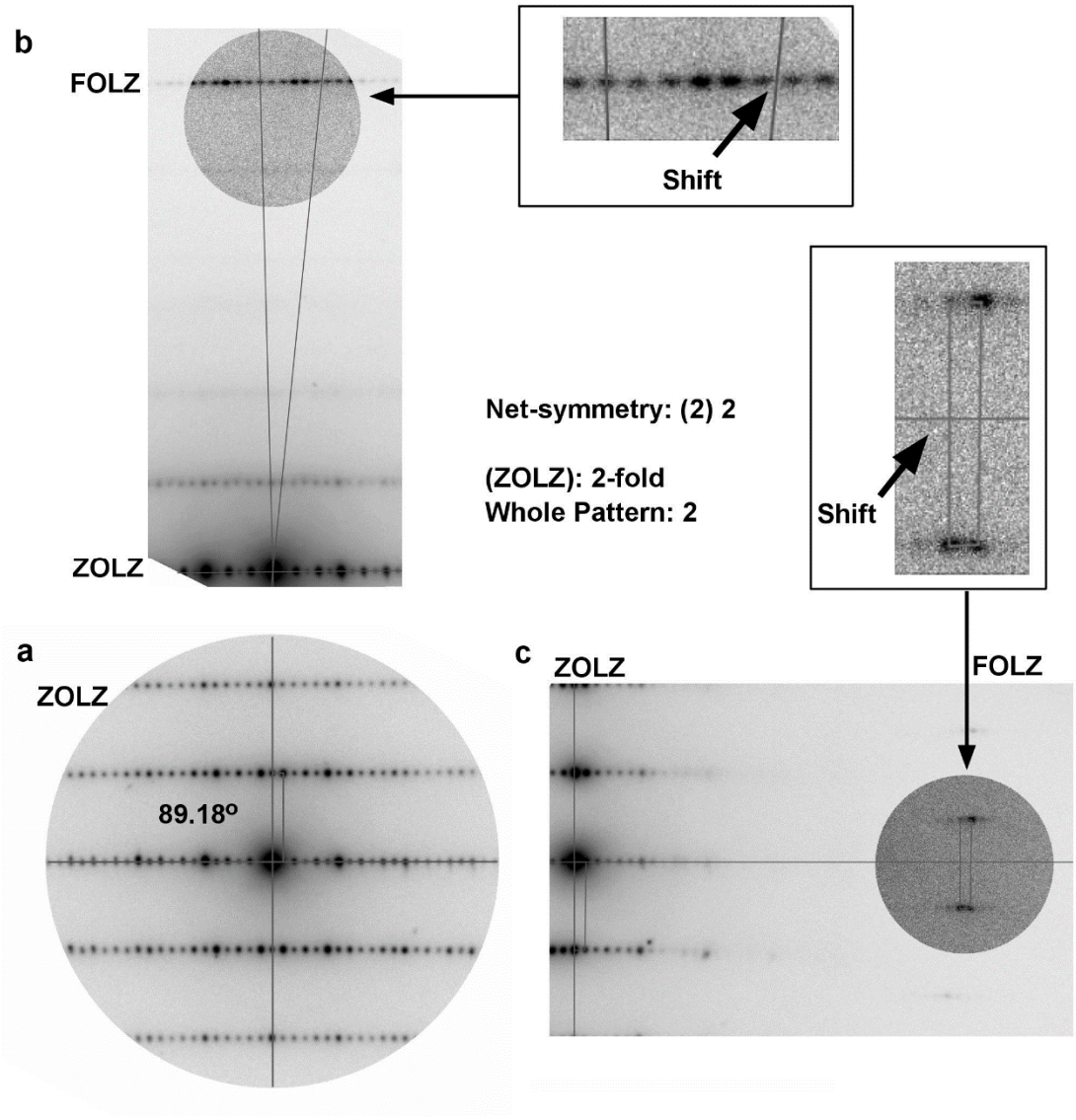

Figure 7 – Electron diffraction of the either $[010]_b$ or $[001]_c$ zone axis required for the identification of the Bravais lattice for the monoclinic crystal system. (a) Only the ZOLZ reflections are visible. The lines indicate the symmetry axis in the pattern. (b-c) Both ZOLZ and FOLZ reflections are visible after the electron beam had been tilted along each axis shown in (a). The narrow parallelogram drawn in each figure corresponds to the "unit" cell in reciprocal space in the ZOLZ and FOLZ. The relative shift of the "unit" cell in the FOLZ, along each symmetry axis, compared to the ZOLZ is an evidence for a non-primitive crystal system. There is no periodicity difference between ZOLZ and FOLZ reflections.